Electronic States and Potential Energy Surfaces of NbC_2

Dingguo Dai,[†] S. Roszak,[†,‡] and K. Balasubramanian*[,†]

Department of Chemistry and Biochemistry, Arizona State University, Tempe, Arizona 85287-1604 and Institute of Physical and Theoretical Chemistry, Wroclaw University of Technology, Wyb. Wyspianskiego 27, 50-370 Wroclaw, Poland

Received: January 21, 2000; In Final Form: March 27, 2000

Potential energy surfaces for the low-lying electronic states of NbC_2 have been computed using the complete active space multiconfiguration self-consistent field (CASMCSCF) followed by the multireference singles + doubles configuration interaction (MRSDCI) calculations that included up to 2.1 million configurations. The density function theory (DFT) was also employed to study several electronic states of NbC_2 near their minima. The DFT results are found to be in good agreement with the CASSCF/MRSDCI results not only for the ground state but also for several excited states, especially with regard to the equilibrium geometries. The dipole moments, vibrational frequencies, and thermodynamic properties are reported. We find a $^4B_1$ state as the ground state of NbC_2 with an isosceles triangular equilibrium geometry and dissociation energy of 5.58 eV. The nature of bonding is discussed using the wave function composition and the Mulliken population analysis. The spin−orbit effects were estimated for the ground state.

I. Introduction

Transition metal carbides have been the subject of many experimental and theoretical studies.[1−40] A primary motivation for these studies is that the transition metal catalysts are extensively employed in reforming petroleum-based products, and thus our comprehension of metal−carbon bonds could aid in the understanding of catalytic selectivity and mechanism. These studies could also provide insight into how the reactivity and bonding vary as a function of the metal. Diatomic and triatomic transition metal carbides offer relatively smaller units to study not only the ground states of these species but also several excited electronic states. Triatomic carbides offer relatively small units to comprehend the bent and bridged C−M−C bonds contained in larger systems, while diatomic transition metal carbides have been the subject of many investigations. The diatomic metal carbides provide a rich array of electronic states for high-resolution laser spectroscopic studies that can probe not only the ground states of these species but also several excited electronic states. On the other hand, there is also significant interest on larger transition metal carbon clusters such as metallofullerenes,[1] metallocarbohedranes, and unusually stable "metcars"[39] as these species exhibit unusual stability and bonding characteristics with potential industrial applications.

Experimental studies on transition metal carbides have a rich history starting with studies made using the Knudsen effusion technique combined with mass spectrometry.[4−7] The earlier studies have yielded atomization energies and thermodynamic properties of these species. Recent studies have included the ion drift tube technique,[2,9−11] electron spin resonance spectroscopy[14−17] of rare-gas matrix-isolated carbides, and high-resolution optical spectroscopy.[12,13,18−23] Larger carbide clusters such as LaC_n^{+2} and $TaC_n^{+3,40}$ have been studied for several values of *n*. A variety of optical spectroscopic techniques have been employed on diatomic carbides containing second-row transition metal atoms such as YC,[13] NbC,[12] and PdC.[19] Photoelectron spectroscopy of the anion has also yielded information on the neutral WC.[18] Matrix-isolated ESR spectroscopy has been utilized on second-row transition metal carbides.[14−17]

The experimental studies related to the title molecule include the matrix-isolated ESR spectroscopy of NbC by Yamrick and Weltner.[14] This study has yielded information on the ground state of the diatomic NbC and its spin multiplicity. Simard and co-workers[12] have obtained the optical spectra of NbC,[12] which have yielded the spectroscopic constants of several low-lying electronic states of the diatomic NbC.

There are several theoretical studies on second-row transition metal carbides such as YC,[8] MoC,[35] RuC,[34] RhC,[30] and PdC.[32,33,36−38] The earlier studies have been typically made using the Hartree−Fock/configuration interaction (HF/CI) techniques.[8,32−35] The RhC[34] and PdC[38] diatomics have been studied using complete active space MCSCF (CAS-MCSCF) followed by multireference configuration interaction (MRSDCI) techniques. Among the triatomics containing transition metal atoms, WC_2[31] and WN_2[49] have been theoretically studied.

Despite many theoretical studies on some of the carbides such as PdC,[32,33,36−38] the relative ordering of the electronic states often remains uncertain, as different levels of theory do not always yield the same information. This is primarily due to the fact that transition metal carbides exhibit a large number of low-lying electronic states of different spin multiplicities and spatial symmetries. While spin exchange stabilization favors the high-spin electronic states, electron correlation effects stabilize the low-spin electronic states, and thus the competition between the two stabilization features place the electronic states at different relative energies at different levels of theory. In addition relativistic effects[41] seem to make significant contributions to the second- and third-row transition metal carbides.

The above survey reveals continued and significant interest in transition metal carbides. While the NbC diatomic has been observed experimentally, it appears that the triatomic NbC_2 has not been studied theoretically at the level of theory employed here. On the basis of the experimental observation of NbC, it

* To whom correspondence should be addressed at kbalu@asu.edu.
† Arizona State University.
‡ Wroclaw University of Technology.

10.1021/jp0002749 CCC: $19.00
Published on Web 05/24/2000

is clear that NbC_2 is a very interesting and potential candidate for future experimental studies. The NbC_2 carbide also has intrinsic theoretical interest as it exhibits a large number of low-lying quartet and doublet electronic states and the nature of bonding in these states seems to differ relative to the participation of Nb(4d), Nb(5s), and Nb(5p). In addition the existence of both open-shell quartet and doublet electronic states makes NbC_2 a prime candidate for matrix-isolated ESR spectroscopy. It appears that a rigorous comparison of the density functional theory (DFT) and CASSCF/MRSDCI techniques would be valuable, especially for the excited electronic states of transition metal carbides. The objectives of the current study include computation of the potential energy surfaces, equilibrium geometries, dipole moments, and spectroscopic properties of the triatomic NbC_2 carbide. We have investigated several low-lying high-spin and low-spin electronic states at the CASSCF and MRSDCI levels that included up to 2.1 million configurations. We have also carried out computations at the DFT level for the low-lying electronic states to facilitate comparison of the DFT and CASSCF/MRSDCI techniques. We have computed the thermodynamic properties (enthalpies and Gibbs free energies) and the vibrational frequencies. The spin−orbit splittings are estimated on the basis of the Nb atomic spin−orbit splittings.

II. Method of Calculation

We have employed three different theoretical techniques to study the electronic states of NbC_2. The complete active space multiconfiguration self-consistent-field (CASSCF) technique was followed by the multireference singles + doubles configuration interaction (MRSDCI) scheme. The results obtained using the Davidson correction for uncoupled quadruple clusters were labeled MRSDCI+Q. We also employed the DFT technique in conjunction with Becke's[50] three-parameter hybrid method using the LYP correlation functional (B3LYP). Geometries of the low-lying electronic states were optimized at the B3LYP, CASSCF, and MRSDCI levels, while the vibrational frequencies were calculated at the B3LYP level.

The computations were carried out using relativistic effective core potentials (RECPs) for the Nb atom taken from La John et al.,[42] which retained the outer $4s^24p^64d^45s^1$ shells of the niobium atom in the valence space replacing the remaining core electrons by RECPs. The RECPs for the carbon atom retained the outer $2s^22p^2$ shells in the valence space. The optimized valence (5s5p4d) Gaussian basis sets for the Nb atom were taken from ref 42. The (4s4p) optimized Gaussian basis sets for the carbon atoms were contracted to (3s3p). The carbon basis sets were supplemented with a set of six-component 3d functions with $\alpha_d = 0.75$. Our final basis sets are (5s5p4d) for the Nb atom and (3s3p1d) for the carbon atoms. In a previous investigation on a related WCO molecule,[48] we have studied the effect of 4f functions. It was found that the inclusion of 4f functions changes the M−C bond lengths by 0.01 Å and bond relative energy separations by 0.01−0.1 eV. Hence in the present study 4f functions were not included in the basis set.

The NbC_2 molecule was computed in the C_{2v} point group placing the molecule on the *yz* plane and the *z* axis chosen as the C_2 axis. Separate CASMCSCF calculations for electronic states of different spatial symmetries and spin multiplicities in the C_{2v} point group were carried out. The C−W−C apex angles were varied from 20° to 180°. For each apex angle, the two equal sides of the isosceles triangle were optimized.

The four orbitals that correspond to the 4s and 4p orbitals of the Nb atom that correlated into two a_1, one b_2, and one b_1 orbitals were kept inactive in that no excitations from these shells were allowed but these orbitals were allowed to relax. Among the remaining orbitals, five a_1, two b_2, two b_1, and one a_2 orbitals (C_{2v} group) were included in the active space. Thirteen valence electrons were distributed in all possible ways among these active orbitals. This choice of active and inactive spaces can be labeled as $n_a = 5, 2, 2, 1$ (a_1, b_2, b_1, a_2) for the active space and $n_i = 2, 1, 1, 0$ for the inactive space. We also computed the dissociation energy of NbC_2 as a supermolecular computation by setting the Nb−C bond lengths as 10 Å.

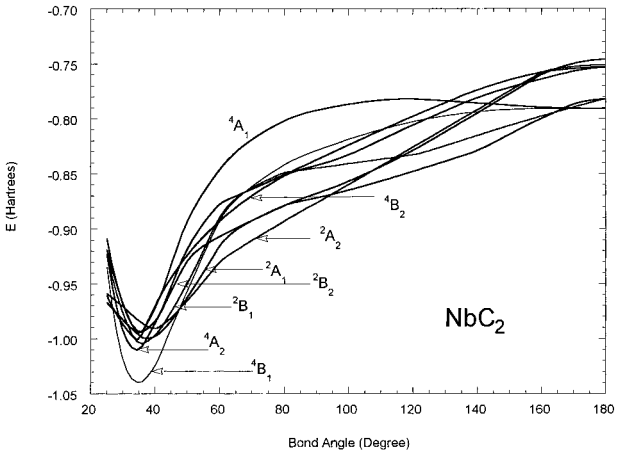

Figure 1. Bending potential energy surfaces for low-lying electronic states of NbC_2.

Following the CASMCSCF calculations, the MRSDCI calculations were carried out for all of the low-lying quartet, doublet, and sextet electronic states of NbC_2 to include the effects of higher order electron correlation. The reference configurations for the MRSDCI computations were chosen from the CASMCSCF calculations with absolute coefficients ≥0.07. All possible single and double excitations were allowed at the MRSDCI. The MRSDCI computations included up to 2.1 million configuration spin functions (CSFs).

We computed the vibrational frequencies of the $^4B_1$ state at the DFT/B3LYP level of theory. For this purpose we started with spin unrestricted Hartree−Fock (UHF) computation of this state followed by the UB3LYP geometry optimization and frequency computation. The UB3LYP computations were made with the Gaussian 98 codes.[51]

The spin−orbit effects were estimated on the basis of the Nb atomic spin−orbit splittings[52] and the contribution of the Nb orbitals to the open-shell orbitals of NbC_2. The contributions become small if the carbon orbitals make substantial contribution to the open-shell orbitals since the spin−orbit effects on the carbons[52] are less than 100 cm^{-1}.

All CASMCSCF/MRSDCI calculations were made using a modified version[46] of ALCHEMY II codes[45] to include the RECPs. The DFT computations were carried out using the Gaussian 98 package of codes.[51]

III. Results and Discussion

Figure 1 shows the bending potential energy surfaces for the quartet and doublet electronic states of NbC_2 as a function of the C−Nb−C apex angles. The sextet electronic states are considerably higher in energy and are thus not shown in Figure 1. For each apex angle, the Nb−C sides of the isosceles triangle were optimized and the optimized energies for the various states are plotted in Figure 1. Table 1 shows the actual equilibrium geometries and the relative energy separations of the bound electronic states of NbC_2 at four different levels of theory,

TABLE 1: Geometries and Energy Separations of the Bent Electronic States of NbC_2

	DFT(B3LYP)				CASMCSCF				MRSDCI			
state	θ^a (deg)	Nb−C (Å)	C−C (Å)	E (eV)	θ^a (deg)	Nb−C (Å)	C−C (Å)	E (eV)	θ^a (deg)	Nb−C (Å)	C−C (Å)	E^b (eV)
$^4B_1$	38.3	2.006	1.315	0.00	38.0	2.005	1.306	0.00	39.6	1.971	1.335	0.00 (0.00)
$^4A_2$	35.3	2.096	1.272	0.63	36.5	2.050	1.284	0.13	36.8	2.040	1.286	0.45 (0.62)
$^2B_1$	38.7	1.992	1.320	0.41	39.6	1.972	1.336	0.89	39.9	1.966	1.342	0.61 (0.55)
$^4B_2$	36.5	2.074	1.299	0.84	37.4	2.041	1.307	0.49	37.9	2.029	1.317	0.72 (0.82)
$^2A_2$	42.7	1.926	1.402	1.01	40.2	1.965	1.352	1.06	41.7	1.948	1.388	0.84 (0.76)
$^2A_1$	37.1	2.015	1.283	1.28	39.8	1.994	1.357	0.91	40.5	1.980	1.371	0.87 (0.80)
$^4A_1$	36.5	2.072	1.298	1.02	37.0	2.047	1.299	0.82	38.0	2.023	1.317	0.88 (0.87)
$^2B_2$	38.0	2.012	1.310	1.09	38.7	1.996	1.323	0.85	39.1	1.987	1.330	1.15 (1.08)
$^6A_2$					34.0	2.244	1.312	1.05	34.6	2.223	1.322	1.81 (2.08)
$^6B_1$	34.0	2.028	1.292	1.79	35.0	2.179	1.310	2.05	36.0	2.147	1.327	2.00 (2.12)
$^6A_1$					34.2	2.220	1.306	1.94	35.2	2.187	1.323	2.14 (2.28)
$^6B_2$					33.8	2.272	1.321	1.99	34.6	2.258	1.343	3.06 (3.44)

[a] Stands for C−Nb−C apex angle. [b] The values in parentheses are Davidson corrected energies.

namely, DFT/B3LYP, CASMCSCF, MRSDCI, and MRSDCI+Q. The MRSDCI+Q results are shown in parentheses for the energy separations.

As seen from Table 1, the CASSCF method predicts very reasonable geometries for the electronic states of NbC_2 with Nb−C bond lengths within 0.06 Å and C−C bond lengths within 0.02 Å of the MRSDCI level, which included dynamical electron correlation effects. A similar comment can be made on the DFT and CASSCF geometries. However, since the CASSCF method includes electron correlation effects only to zero-order, it does not include dynamical electron correlation effects. Thus the energy separations which are sensitive to the dynamical electron correlation effects tend to have greater impact on the energy separations of the electronic states. For example, the $^4A_2-^4B_1$ energy separation is only 0.13 eV at the CASSCF level, while it becomes 0.45 and 0.62 eV at the MRSDCI and MRSDCI+Q levels, respectively. On the other hand, the $^2B_1$ state is predicted to be higher at the CASSCF level compared to the MRSDCI and MRSDCI+Q levels. The same comment is applicable to other doublet electronic states, as seen from Table 1. This is consistent with the fact that electron correlation effects tend to stabilize the low-spin electronic states relative to the high-spin states, and thus higher levels of theory lower the doublet electronic states.

As seen from Table 1, the ground state of NbC_2 is predicted to be the $^4B_1$ state with a very acute isosceles triangular geometry, although at the CASSCF level the $^4A_2$ state is a viable candidate. The $^4B_1$ ground state has relatively short Nb−C bonds compared to the sextet states, but the doublet states have shorter Nb−C bond lengths as expected. The shortest Nb−C bonds are exhibited by the $^2A_2$ state. It is also interesting that the relative ordering of the $^4A_2$ and $^2B_1$ states changes at the MRSDCI+Q level, suggesting that the low-spin doublet state is stabilized at the higher order level of electron correlation. As seen from Table 1, all sextet electronic states are considerably higher. The Nb−C bond lengths are longer for the sextet states as expected compared to the low-spin states.

As evidenced from Table 1, the DFT/B3LYP results are in good agreement with the MRSDCI results, which are more CPU-intensive. Most of the electronic states considered in Table 1 are dominated by single reference configuration, and thus the DFT method should provide a very good description of the electronic states. The DFT geometries are quite close to the MRSDCI geometries with Nb−C bond distances within 0.06 Å and C−C bond distances within 0.02 Å for most of the states. More importantly, the relative energy separations at the DFT level are quite similar to the MRSDCI+Q results, although at the MRSDCI level there are some differences, for example, with the $^2B_1$ state. On the other hand, there are other notable differences as seen from Table 1. For example, the $^2A_1$ excited state is predicted to be at 1.28 eV higher than $^4B_1$ at the DFT level, but the MRSDCI level predicts this state to be only 0.87 eV higher than $^4B_1$ and the MRSDCI+Q level stabilizes this state further. In fact the DFT level places the $^2A_1$ state higher than $^4A_1$, while an opposite trend is predicted at the MRSDCI and MRSDCI+Q levels. With the exception of these variations, the DFT and MRSDCI techniques seem to be in good accord.

As seen from Figure 1, the bending potential energy surfaces of the electronic states of NbC_2 exhibit crossings of the doublet and quartet electronic states. The spin−orbit coupling between the states could be interesting in the region of the curve crossings, but the crossings generally occur substantially away from the minima, and thus they would not have large impact near the minima. As seen from Figure 1, all of the electronic states of NbC_2 exhibit very acute apex angles between 35° and 43°. This is consistent with the short C−C bonds seen in Table 1. All of the electronic states also exhibit isosceles triangular structures consistent with Table 1.

The vibrational frequencies were computed using the density functional level of theory in conjunction with the B3LYP potentials. The A_1 symmetric stretch vibrational frequency was computed as 1569 cm^{-1}, while the B_2 asymmetric and A_1 "bending mode" frequencies were computed as 301 and 577 cm^{-1}, respectively. Note that the conventional way of looking at the A_1 bending mode for a bent C_{2v} molecule is not applicable for NbC_2 due to the strong C−C bonding at the base of the isosceles triangle, and thus bending the apex angle would result in C−C stretch at the base. For this reason, in fact the low-frequency A_1 mode is the strongest of all three modes. The IR intensities of the low-frequency and high-frequency A_1 modes are 53.1 and 0.7, respectively, while the B_2 asymmetric stretch has an IR intensity of 2.2.

We calculated the dissociation energy to separate NbC_2 into Nb and C_2. At the CASMCSCF level, we computed the dissociation energy (D_e) as 4.07 eV, while at the higher MRSDCI and MRSDCI+Q levels this value becomes 5.58 and 5.83 eV, respectively. The same basis set for C was used before to compute the D_e of C_2 as 5.95 eV at the second-order CI (SOCI) level compared to the well-known experimental D_e of C_2, which is 6.21 eV.[47] We obtain the atomization energy of NbC_2 as 12.0 eV by combining the dissociation energies of the two species. The zero-point correction for NbC_2 is computed as 3.5 kcal/mol.

Table 2 shows the computed thermodynamic properties of NbC_2 at two different levels of theory, namely the DFT and CASSCF levels. The properties shown include the Gibbs free energies and enthalpies at several temperatures. As seen from Table 2, the CASSCF and DFT results are quite close to each

TABLE 2: Gibbs Energy Function (GEF) and Heat Constant Function (ΔH) Calculated for the Ground $^4B_1$ State of NbC_2 as a Function of Temperature

T (K)	298.15	2000	2200	2400	2600	2800	3000
GEF (J/mol K)	−243.1	−329.5	−334.5	−339.1	−343.3	−347.3	−351.0
ΔH (kJ/mol)	11.5	103.8	115.3	126.7	138.3	149.8	161.3

TABLE 3: Dipole Moment for the Bent Minimum of NbC_2

state	μ,[a] D	state	μ,[a] D
$^4B_1$	5.99	$^4A_1$	6.75
$^4A_2$	6.71	$^2B_2$	5.80
$^2B_1$	5.72	$^6A_2$	3.10
$^4B_2$	5.78	$^6B_1$	3.37
$^2A_2$	7.43	$^6A_1$	3.03
$^2A_1$	7.28	$^6B_2$	4.20

[a] Polarity is Nb^+C^-.

other. The thermodynamic properties can be compared with the experimental values when they become available.

Table 3 shows the dipole moments of the low-lying electronic states of NbC_2 at their equilibrium geometries. As seen from Table 3, the electronic states of NbC_2 exhibit large dipole moments with Nb^+C^- polarity of bonds consistent with their ionic bonding and transfer of electronic charge from Nb to the carbon atoms. With the exception of the $^2B_1$ state, the doublet electronic states have substantially larger dipole moments with the $^2A_2$ state exhibiting the largest dipole moment. The $^4B_1$ ground state exhibits a relatively large dipole moment of 5.99 D. The polarity of the Nb−C bonds are Nb^+C^-, and the overall dipole vector points in the $+z$ direction (NbC_2 on the *yz* plane with *z* axis bisecting the C−Nb−C apex angle). The sextet electronic states have much smaller dipole moments due to smaller charge transfer from Nb to C in high-spin electronic states. The large dipole moments of the electronic states of NbC_2 are also consistent with very acute apex angles exhibited by these states. For a given spin multiplicity, the dipole moments seem to correlate with the Nb−C bond distances for a given amount of charge transfer. For electronic states of the same spin multiplicity, the longer the Nb−C bond distances are the larger are the dipole moments. However, for higher spin states such as the sextet states, the charge transfer from Nb to C is smaller, although the Nb−C bond distances are longer thus explaining the smaller dipole moments.

The large dipole moments combined with very acute triangle structures exhibited by the low-lying electronic states would suggest that NbC_2 bonding in these states could be described by Nb^+ bound to C_2^-. This is further confirmed by our computed C−C bond length 1.286−1.34 Å, which compares with the C−C bond distance of 1.268 Å reported by Maier and Rosslein[53] for C_2^- for the $^2\Sigma_g^-$ ground state. Thus the bonding could be described as Nb^+ bound side-on to C_2^- with electronic back transfer from C_2^- to Nb^+.

IV. The Bonding Nature of the Low-Lying States of NbC_2

We have analyzed the nature of bonding in NbC_2 through the composition of the orbitals, the leading configurations, and the Mulliken populations. The extent of charge transfer from Nb to C and back transfer from C to Nb can be rationalized through the total Mulliken populations, while the individual Mulliken populations provide insight into the extent of participation of the 5s, 5p, and 4d orbitals of the Nb atom.

Table 4 shows the leading configurations and their coefficients for the low-lying electronic states of NbC_2 in the MRSDCI wave functions. As seen from Table 4, almost all of the electronic states of NbC_2 are predominantly composed of a single configuration with coefficients >0.91. Note that although there

TABLE 4: Leading Configurations of the Electronic States of NbC_2 in the MRSDCI Wave Functions[a]

		configurations						
state	coefficient	$5a_1$	$6a_1$	$7a_1$	$3b_2$	$2b_1$	$3b_1$	$1a_2$
$^4B_1$	0.915	2	1	0	1	2	0	1
$^4A_2$	−0.910	2	1	1	0	2	0	1
$^2B_1$	−0.860, −0.264	2	1	0	1	2	0	1
$^4B_2$	−0.917	2	1	1	1	2	0	0
$^2A_2$	0.906	2	0	0	2	2	0	1
$^2A_1$	−0.903	2	1	0	2	2	0	0
$^4A_1$	−0.918	2	0	0	1	2	1	1
$^2B_2$	−0.905	2	2	0	1	2	0	0
$^6A_2$	−0.920	1	1	1	1	2	1	0
$^6B_1$	0.929	1	1	1	1	2	0	1
$^6A_1$	0.933	1	1	0	1	2	1	1
$^6B_2$	0.941	2	1	1	1	1	1	0

[a] The $(1a_1)^2...(4a_1)^2(1b_2)^2(2b_2)^2(1b_1)^2$ is common to all the electronic states.

are two CSFs contributing to the $^2B_1$, state they originate from the same electronic distribution, and it is thus single reference in character.

The fact that all of the states are single reference in character may explain the agreement of the DFT method with the MRSDCI method. As seen from Table 4, the $^4A_2$ state arises from the promotion of an electron from the $3b_2$ to $7a_1$ orbitals relative to the $^4B_1$ state. On the other hand, as seen from Table 4, the $^4A_1$ state arises from the excitation of the $6a_1$ electron to the $3b_1$ orbital. Likewise some states involve promotion of $1a_2$ to $3b_1$ or $1a_2$ to $7a_1$. It is thus useful to analyze the compositions of these orbitals to gain further insight into the electronic states of these species.

The high-lying occupied orbitals and the low-lying unoccupied orbitals of NbC_2 can be analyzed using the $^4B_1$ ground state. The $^2A_2$ state may also be used as it is the lowest doublet state with a different electronic configuration, thus providing a doubly occupied $3b_2$ orbital for the analysis. The singly occupied $3b_2$ orbital of the $^4B_1$ state is mainly composed of $Nb(4d_{yz}) + C_1(2s) - C_2(2s) - C_1(2p_z) + C_2(2p_z)$, while the same orbital of the $^2A_2$ state (doubly occupied) has smaller contribution from $Nb(4d_{yz})$ and larger contributions from the 2s and $2p_z$ orbitals of the carbons. The singly occupied $6a_1$ orbital of the $^4B_1$ state is composed almost fully of $Nb(4d_{x^2-(y^2+z^2)}) - Nb(5s)$, with substantially smaller contributions from carbons. Again in the case of the $^2A_2$ state, this orbital is the lowest unoccupied molecular orbital (LUMO) with increased carbon contribution, and it is composed of $Nb(4d_{z^2-(x^2+y^2)}) + Nb(5s) - C_1(2s) - C_2(2s) + C_1(2p_y) - C_2(2p_y) - C_1(2p_z) - C_2(2p_z)$.

In general, if the overall compositions of two electronic states are nearly same, their apex bond angles are also similar. For example, the leading configurations of the $^4B_1$ and $^2B_1$ states are the same as seen from Table 4. Their equilibrium bond angles are 39.6° and 39.9°, respectively (Table 1). However, the $^6B_1$ ground state has two singly occupied $5a_1$ and $7a_1$ orbitals instead of a doubly occupied $6a_1$ orbital for the $^4B_1$ and $^2B_1$ states, and hence its apex bond angle differs (36.0°) at the MRSDCI level.

Figure 2 shows the pictorial representation of the highest orbitals of NbC_2. As some of these orbitals are somewhat complex, it is useful to have pictorial representations. These figures provide further insight into the nature of these orbitals.

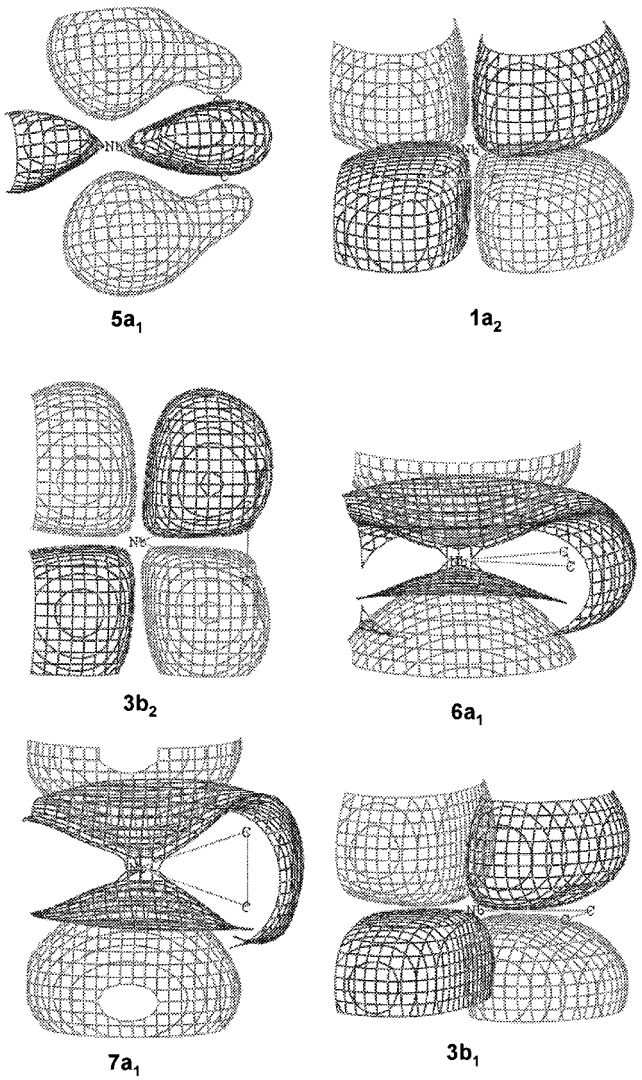

Figure 2. Plots of some of the high-lying occupied ($5a_1$, $1a_2$, $3b_2$, $6a_1$) and the lowest unoccupied ($7a_1$ and $3b_1$) orbitals of NbC_2.

The orbitals plotted in these figures are for the $^4B_1$ ground state near its global minimum. The first four orbitals are occupied orbitals while the last two orbitals are unoccupied. The $6a_1$ orbital is the HOMO while $7a_1$ is LUMO. As seen from Figure 2, the descriptions of the orbitals as outlined above are consistent with the orbital plots in that the $1a_2$ and $3b_1$ orbitals have significant $d\pi$ or $d\delta$ contributions from the Nb atom. The $3b_2$ orbital is a strong mixture of Nb($4d_{yz}$), $C_1(2s) - C_2(2s)$, and $C_1(2p_z) + C_2(2p_z)$, while the $5a_1$, $6a_1$, and $7a_1$ orbitals are significant mixtures of Nb and C orbitals.

Table 5 shows the Mulliken populations of the electronic states of NbC_2 which clearly show the involvement of the niobium and carbon orbitals and electron transfer in the bonding of NbC_2. As seen from Table 5, the niobium atom has a Mulliken population between 4.35 and 4.53, while each of the two carbon atoms has a gross population between 4.23 and 4.32. Since the atomic configuration of the Nb atom is (core)$4d^45s^1$, a strong deviation from a gross Nb population of 5.0 clearly suggests significant electron transfer from the niobium atom to the carbon atoms. As seen from Table 5, the 5s populations of the niobium atom for the electronic states are between 0.68 and 0.81, while the 4d populations are between 3.3 and 3.9. The 5p populations of the niobium atom are between 0.17 and 0.31. It is therefore evident that the Nb deviates strongly from its natural atomic population in two ways: first due to charge transfer from Nb to carbons and also due to rearrangement of the atomic populations among 5s, 5p, and 4d orbitals. The significant reduction in the 5s populations of Nb is primarily due to charge transfer to carbons and also due to the increase in the 5p and 4d populations of Nb. It is quite interesting that the 4d orbital does not participate in the charge-transfer process in contrast to some third-row transition metal carbides,[31] which exhibit charger transfer from 5d. This contrast is primarily due to relativistic effects,[41] which stabilize the 6s orbital and destabilize the 5d in the case of third-row transition metal carbides. For the carbon atoms, all 2s orbitals have populations less than 1.83, while the 2p populations are more than 2.4. The variations from their pure atomic populations are due to both hybridization and charge transfer from Nb.

TABLE 5: Mulliken Population Analysis for the Electronic States of NbC_2[a]

	gross population						
state	Nb	C[b]	Nb(s)	Nb(p)	Nb(d)	C (s)[b]	C (p)[b]
$^4B_1$	4.398	4.301	0.747	0.180	3.471	1.718	2.526
$^4A_2$	4.425	4.288	0.684	0.165	3.576	1.653	2.580
$^2B_1$	4.440	4.280	0.708	0.193	3.539	1.668	2.555
$^4B_2$	4.396	4.302	0.810	0.253	3.333	1.728	2.518
$^2A_2$	4.394	4.303	0.274	0.191	3.929	1.778	2.569
$^2A_1$	4.402	4.299	0.624	0.198	3.580	1.749	2.495
$^4A_1$	4.352	4.324	0.264	0.308	3.780	1.677	2.593
$^2B_2$	4.457	4.272	0.942	0.166	3.349	1.666	2.550
$^6A_2$	4.448	4.276	0.709	0.281	3.458	1.629	2.600
$^6B_1$	4.534	4.233	0.738	0.207	3.589	1.622	2.562
$^6A_1$	4.450	4.275	0.733	0.287	3.430	1.615	2.613
$^6B_2$	4.442	4.279	0.774	0.254	3.414	1.826	2.403

[a] The $5s^25p^6$ shells for Nb are not included. [b] Represents one of the two equivalent C atoms.

The $^4B_1$ state for NbC_2 is composed of Nb($4d^{3.471}5s^{0.747}5p^{0.18}$) and C($2s^{1.718}2p^{2.526}$). Since this state arises from the Nb($4d^35s^2$)^{4}F atom, the populations can be compared with the atomic state to deduce the extent of charge transfer and hybridization. In the $^4B_1$ state carbon transfers 0.282*e* electron density from its 2s orbital, the C(2p) orbital accepts 0.526*e*, while niobium donates 1.253*e* from its 5s orbital and it receives 0.471*e* in its 4d orbital. Thus analogous to other transition metal carbides, it can be rationalized that the formation of the Nb−C bonds is assisted by charge transfer from the 5s orbital of niobium atom to the 2s orbital of carbon and back transfer from C(2p) to Nb(5p) and Nb(4d) through the dative $p\pi-d\pi$ and $p\pi-p\pi$ bonds.

It may be seen from Table 5 that the Mulliken populations vary substantially among the various electronic states. For example, the $^2A_2$ state of NbC_2 exhibits a substantially larger Nb(4d) population of 3.93, a Nb(5s) population of only 0.27, and a Nb(5p) population of 0.2. However, the overall charge transfer from Nb to the carbons is quite comparable to the $^4B_1$ ground state, and thus the difference should be viewed as primarily due to the difference in the participation of the 4d versus 5s orbitals in the bonding. This is also consistent with the substantial difference in the geometry of the $^2A_2$ state of NbC_2, which exhibits significantly shorter Nb−C bonds and thus a larger C−Nb−C apex angle, as seen from Table 1. The differences between the various electronic states can thus be rationalized on the basis of individual orbital participation. As seen from Table 5, the high-spin states exhibit greater total Nb populations suggesting smaller charge transfers to the carbon atoms. This is fully consistent with the smaller dipole moments of these states relative to the low-spin states.

The spin−orbit splittings of NbC_2 can be estimated from the atomic Nb splitting.[52] As seen from the atomic data, the Nb ^{6}D($4d^45s^1$) ground state splits into $J = {}^1/_2$, ${}^3/_2$, ${}^5/_2$, ${}^7/_2$, and ${}^9/_2$

atomic states with a total splitting of 1050 cm^{-1} between the highest and lowest J states. On the other hand, the $^4F(4d^35s^2)$ spin−orbit splitting is 1663 cm^{-1}. The Nb Mulliken populations of the ground state are closer to the $4d^45s^1$ configuration than the $4d^35s^2$. In fact, the charge transfer from Nb to C reduces the Nb 4d and 5s populations compared to the ground state of atomic Nb. The ground state of NbC_2 correlates into two $E_{1/2}$ states in the double group[41] of C_{2v}. Thus the splitting between the two $E_{1/2}$ states would become smaller due to the coalescence of different J states of Nb. The spin−orbit splitting of NbC_2 comes primarily from the open-shell $6a_1$, $3b_2$, and $1a_2$ orbitals. Although the $6a_1$ and $1a_2$ orbitals are significantly Nb in character, the $3b_2$ orbital is a mixture of Nb(4d), C(2s), and C(2p). The contributions from Nb(4d) and C(2p) are quite significant in the $3b_2$ orbital. Therefore the spin−orbit splitting is expected to be quenched further by the participation of the C(2s) and C(2p) orbitals in the $3b_2$ open-shell orbital of NbC_2. On the basis of the atomic orbital contributions to the open-shell orbitals of NbC_2 and the Nb Mulliken populations, we estimate the splitting between the two $E_{1/2}$ states of NbC_2 to be about 400 cm^{-1}.

V. Conclusion

The bending potential energy surfaces of NbC_2 were reported for both quartet and doublet electronic states. The ground state of NbC_2 was found to be a high-spin $^4B_1$ state. The equilibrium geometry of the ground state was found to be a very acute isosceles triangle with Nb−C bond lengths of 2.066 Å and C−Nb−C apex angle of 36.8°. In addition, we found four doublet and three other low-lying quartet electronic states and high-lying sextet states for NbC_2 with isosceles triangular equilibrium geometries. The dipole moments of all the electronic states reveal strong ionic bonding with Nb^+C^- polarity. The vibrational frequencies of the $^4B_1$ state are reported. The thermodynamic functions such as the Gibbs free energies and enthalpies were computed for several temperatures. The nature of bonding of the low-lying electronic states for NbC_2 is discussed through the leading configurations, orbital compositions, and the Mulliken populations. The formation of the Nb−C bonds is assisted by significant charge transfer from Nb to the carbons followed by smaller back transfer from C to Nb with $d\pi-p\pi$ and $p\pi$-$p\pi$ bonds. The spin−orbit splitting of the $^4B_1$ state was estimated.

Acknowledgment. This research was supported by the U.S. Department of Energy under Grant DEFG02-86ER13558.

References and Notes

(1) Heath, J. R.; O'Brien, S. C.; Zhang Q.; Liu, Y.; Curl R. F.; Krato, H. W.; Tittel, F. K.; Smalley, R. E. *J. Am. Chem. Soc.* **1985**, *107*, 7779.
(2) Clemmer, D. E.; Shelimov, K. B.; Jarrold, M. F. *J. Am. Chem. Soc.* **1994**, *116*, 5971.
(3) Cassady, C. J.; McElvany, S. W. *J. Am. Chem. Soc.* **1990**, *112*, 4788.
(4) Gingerich, K. A. *J. Less-Common Met.* **1985**, *110*, 41; *Curr. Top. Mater. Sci.* **1980**, *6*, 345.
(5) Gingerich, K. A.; I. Shim, I. In *Advances in Mass Spectroscopy 1985*; Todd, J. F. J., Ed.; Wiley: New York, 1986; p 1051.
(6) Pelino, M.; Haque, R.; Bencivenni, L.; Gingerich, K. A. *J. Chem. Phys.* **1988**, *88*, 6534.
(7) Pelino, M.; Gingerich, K. A.; Haque, R.; Bencivenni, L. *J. Phys. Chem.* **1986**, *90*, 4358.
(8) Shim, I.; Pelino, M.; Gingerich, K. A. *J. Chem. Phys.* **1992**, *97*, 9240.
(9) Shelimov, K. B.; Clemmer, D. E.; Jarrold, M. F. *J. Phys. Chem.* **1995**, *99*, 11376.
(10) Clemmer, D. E.; Shelimov, K. B.; Jarrold, M. F. *Nature* **1994**, *367*, 718.
(11) Shelimov, K. B.Clemmer, D. E.; Jarrold, M. F. *J. Phys. Chem. 1994*, *98*, 12819.
(12) Simard, B.; Presunka, P. I.; Loock, H. P.; Berces, A.; Launila, O. *J. Chem. Phys.* **1997**, *107*, 307.
(13) Simard, B.; Hackett, P. A.; Balfour, W. J. *J. Chem. Phys.* **1997**, *107*, 307.
(14) Hamrick, Y. M.; Weltner, Jr., W. *J. Chem. Phys.* **1991**, *94*, 3371.
(15) Van Zee, R. J.; Bianchini, J. J.; Weltner, Jr., W. *Chem. Phys. Lett.* **1986**, *127*, 314.
(16) Brom, J. M.; Graham, W. R. M.; Weltner, W. Jr., *J. Chem. Phys.* **1972**, *57*, 4116.
(17) Weltner, Jr., W. *Magnetic Atoms and Molecules*; Dover Publications: New York, 1983.
(18) Li, X.; Liu, S. S.; Chen, W.; Wang, L. S. *J. Chem. Phys.* **1999**, *111*, 2464.
(19) Langenberg, J. D.; Shao, L.; Morse, M. D. *J. Chem. Phys.* **1999**, *111*, 4077.
(20) Langenberg, J. D.; DaBell, R. S.; Shao, L.; Dreesen, D.; Morse, M. D. *J. Chem. Phys.* **1998**, *109*, 7863.
(21) Simard, B.; Hackett, P. A.; Balfour, W. J. *Chem. Phys. Lett.* **1994**, *230*, 103.
(22) Barnes, M.; Merer, A. J.; Metha, G. F. *J. Chem. Phys.* **1995**, *103*, 8360.
(23) Roszak, S.; Balasubramanian, K. *J. Chem. Phys.* **1997**, *106*, 158.
(24) Roszak, S.; Balasubramanian, K. *J. Phys. Chem.* **1997**, *101*, 2666.
(25) Roszak, S.; Balasubramanian, K. *Chem. Phys. Lett.* **1997**, *264*, 80.
(26) Roszak, S.; Balasubramanian, K. *Chem. Phys. Lett.* **1997**, *265*, 553.
(27) Majumdar, D.; Balasubramanian, K. *Chem. Phys. Lett.* **1997**, *280*, 212.
(28) Tan, H.; Liao, M. Z.; Balasubramanian, K. *Chem. Phys. Lett*. **1997**, *280*, 219.
(29) Tan, H.; Liao, M. Z.; Balasubramanian, K. *Chem. Phys. Lett*. **1997**, *280*, 423.
(30) Majumdar, D.; Balasubramanian, K. *Chem. Phys. Lett*. **1998**, *284*, 273.
(31) Dai, D. G.; Balasubramanian, K. *J. Phys. Chem. A*, in press.
(32) Shim, I.; Gingerich, K. A. *J. Chem. Phys.* **1982**, *76*, 3833.
(33) Shim, I.; Gingerich, K. A. *Surf. Sci.* **1985**, *156*, 623.
(34) Shim, I.; Finkbeiner, H. C.; Gingerich, K. A. *J. Phys. Chem.* **1987**, *91*, 3171.
(35) Shim, I.; Gingerich, K. A. *J. Chem. Phys*. **1997**, *106*, 8093.
(36) Pacchioni, G.; Koutecky, J.; Fantucci, P. *Chem. Phys. Lett*. **1982**, *92*, 486.
(37) Russo, N.; Andzelm, J.; Salahub, D. R. *Chem. Phys.* **1987**, *114*, 331.
(38) Tan, H.; Dai, D.; Balasubramanian, K. *Chem. Phys. Lett.* **1998**, *286*, 375.
(39) Cartier, S. F.; May, M. B.; Castleman, Jr., A. W. *J. Am. Chem. Soc.* **1994**, *116*, 5295.
(40) McElvany, S. W.; Cassady, C. J. *J. Phys. Chem.* **1990**, *94*, 2057.
(41) Balasubramanain, K. *Relativistic Effects in Chemistry. Part A: Theory and Techniques*; Wiley-Interscience: New York, 1997; p 301; *Relativistic Effects in Chemistry. Part B: Applications*; Wiley-Interscience: New York, 1997; p 531.
(42) La John, L. A.; Christiansen, P. A.; Ross, R. B.; Atashroo, T.; Ermler, W. C. *J. Chem. Phys*. 1**987**, *87*, 2812.
(43) Balasubramanian, K. *J. Chem. Phys.* **1988**, *89*, 5731.
(44) Pitzer, R. M.; Winter, N. W. *J. Phys. Chem.* **1988**, *92*, 3061.
(45) The major authors of ALCHEMY II are Lengsfield, B.; Liu, B.; Yoshmine, Y.
(46) Balasubramanian, K. *Chem. Phys. Lett.* **1986**, *127*, 585.
(47) Huber, K. P.; Herzberg, G. *Molecular Spectra and Molecular Structure IV*, *Constants of Diatomic Molecules*; Van Nostrand Reinhold: New York, 1979.
(48) Tan, H.; Liao, M. Z.; Balasubramanian, K. *J. Phys. Chem. A* **1998**, *102*, 6801.
(49) Pyykkö, P.; Tamm, T. J. *J. Phys. Chem. A* **1997**, *101*, 8107.
(50) Becke, A. D. *J. Chem. Phys*. **1993**, *98*, 5648.
(51) Frisch, M. J.; Trucks, G. W.; Schlegel, H. B.; Scuseria, G. E.; Robb, M. A.; Cheeseman, J. R.; Zakrzewski, V. G.; Montgomery, Jr., J. A.; Stratmann, R. E.; Burant, J. C.; Dapprich, S.; Millam, J. M.; Daniels, A. D.; Kudin, K. N.; Strain, M. C.; Farkas, O.; Tomasi, J.; Barone, V.; Cossi, M.; Cammi, R.; Mennucci, B.; Pomelli, C.; Adamo, C.; Clifford, S.; Ochterski, J.; Petersson, G. A.; Ayala, P. Y.; Cui, Q.; Morokuma, K.; Malick, D. K.; Rabuck, A. D.; Raghavachari, K.; Foresman, J. B.; Cioslowski, J.; Ortiz, J. V.; Baboul, A. G.; Stefanov, B. B.; Liu, G.; Liashenko, A.; Piskorz, P.; Komaromi, I.; Gomperts, R.; Martin, R. L.; Fox, D. J.; Keith, T.; Al-Laham, M. A.; Peng, C. Y.; Nanayakkara, A.; Gonzalez, C.; Challacombe, M.; Gill, P. M. W.; Johnson, B.; Chen, W.; Wong, M. W.; Andres, J. L.; Gonzalez, C.; Head-Gordon, M.; Replogle, E. S.; Pople, J. A. *Gaussian 98*, Revision A.7; Gaussian, Inc.: Pittsburgh, PA, 1998.
(52) Moore, C. E. *Tables of Atomic Energy Levels*; U.S. National Institute of Standards and Technology: Washington, DC, 1971; Vol. II.
(53) Maier, J. P.; Rosslein, M. *J. Chem. Phys.* **1988**, *88*, 4614.